ALGAL BIOPHYSICS: MODELING OF GROWTH KINETICS AND CHARACTERIZATION OF MEMBRANE MECHANICS

_____

A Thesis

Presented to

the Faculty of Natural Sciences and Mathematics

University of Denver

_____

In Partial Fulfillment

of the Requirements for the Degree

Master of Physics

_____

By

Antonio Nava Jr.

August 2012

Advisor: Sean Eric Shaheen

Author: Antonio Nava Jr.
Title: ALGAL BIOPHYSICS: MODELING OF GROWTH KINETICS AND CHARACTERIZATION OF MEMBRANE MECHANICS
Advisor: Sean Eric Shaheen
Degree Date: August 2012

ABSTRACT

One growing field in alternative energy is biofuel production through microorganisms. This field of research includes hydrogen and biofuel production through the cultivation of algae. In this work, we have selected two different algae to study, *Anabaena* sp. cpcc 387 and *Tetraselmis*. Through mathematical modeling of *Anabaena* we investigated the complex multicellular relationships and colony stability when noise is introduced. We developed a mathematical model using a system of differential equations that simulates the population growth through optical density over time of *Anabaena*. When the model was compared to experimental data obtained through growing *Anabaena* in a photobioreactor, we found a strong linear correlation of 0.98 suggesting that the model reasonably simulates the lag, exponential and stationary phase. As a result, the model may be used to study the effects of varying different parameters in *Anabaena's* environment in order to predict what effect it will have on colony growth pattern and population.

In conjunction with researchers at the National Renewable Energy Laboratory, we characterize *Tetraselmis* cells' membrane elasticity. Through use of an Atomic Force Microscope (AFM), varying forces were applied to the cell membrane that was used to find the modulus of elasticity to be 79.8 KPa ± 19.8 and 46.9 KPa ± 2.04 for two different

cells tested. Having found the modulus of two cells is the starting point for collecting more data on this strain and other strains along with various other pretreatments. This will allow for cross comparisons between cell membrane strength and give quantitative evidence for which strain and pretreatment yield the weakest cell membrane to allow to lipid extraction.

Table of Contents

Table of Figures

Chapter One: Introduction and Motivation

Algae are a promising avenue to alternative energy production. To name a few of their uses, algae may be used as a biomass, harvested for lipids toward biofuel production, and used as source for hydrogen production [1,2,3]. A benefit to the use of algae as a renewable energy source is the simple requirements necessary to cultivate algae. Other sources of renewable energy such as switch grass or corn require fertile land to grow; land that could be used to grow crops used for food [4,5]. Algae on the other hand only need water and sunlight to be cultivated, and depending on the strain, this can be salt water [6]. The location and overall agricultural quality of the land are not important, thus arid land that is not suitable as farmland can be used for the purpose of building a facility to cultivate and harvest the algae. The lipids that algae produce can be processed into a biodiesel [7]. Other strains of algae can be grown in order to collect the gases such as Hydrogen that they produce as a byproduct of their photosynthesis.

Biofuels can be produced from a variety of different biomass sources that contain some form of sugar or cellulose [8]. The benefit of an algal source lies in the algae's ability to produce lipids, which can be processed into biofuels through a procedure that requires less processing [9].

The technical hurdles start with successful cultivation. Batches of algae can become contaminated during cultivation by foreign algae, resulting in the starvatio

of the high lipid producing algae due to starvation from the competing invader. Other issues lie in finding efficient methods of extracting lipids from within cells. In order to study what effect different pretreatments have on the strength of the cell wall, we characterize the cell membrane using an AFM. Using the AFM, we apply varying forces to the cell membrane to find an estimate for its modulus of elasticity and rupture point.

Cyanobacteria are a grouping of Gram-negative prokaryote microorganisms that carry out oxygenic photosynthesis to produce its energy [6]. The name derives from their blue-green appearance. Found in a great variety of locations around the world, cyanobacteria have a tremendous ability to adapt to various locals. In fact, fossil records date them back as far as 2.8 billion years [10]. Cyanobacteria are sub classified into cells that can create heterocysts that fix nitrogen [6].

The ability to fix nitrogen becomes important when nitrates become low in the cells environment and provides a new avenue of nitrate collection [10,11,12]. Although, the ability to photosynthesize and produce nitrogen poses an issue wherein oxygen, which is involved in photosynthesis, can bind to the nitrogenese enzyme permanently inactivating a heterocyst's ability to fix nitrogen [13,14]. Cyanobacteria have evolved 2 primary methods to mitigate this issue. By separating the 2 different and incompatible processes through either spatial or temporal division, a single or collection of cells can have access to both photosynthesis and nitrogen fixation [15,16]. In temporal separation, the cell only allows one process to occur at a time such as through the use of a circadian clock or photosynthesizing during daylight and switching over to nitrogen

fixation when light levels have dropped to a low enough level. In spatial division of photosynthesis and nitrogen fixation, the cells involved will contain one process, excluding the other, leading to specialized cells.

Anabaena is a sub classification of Cyanobacteria. Specifically, Anabaena is classified into the family of Nostocaceae, which are filamentous bacteria capable of forming heterocyst cells and can fix nitrogen [6]. Primarily consisting of vegetative cells of about 5 micrometers in size, *Anabaena* can grow in filaments of lengths of dozens of cells, similar to beads on a string. Vegetative cells are the common cell to the algae that form under favorable growing conditions and perform photosynthesis. When a source of combined nitrogen low in its environment, vegetative cells can irreversibly differentiate into heterocyst cells [8,12,13,17]. Once the process is complete, irreversible differentiation into a heterocyst cell is permanent and leads to the cells inability to self-replicate. On average, terminal differentiation of vegetative cells into heterocyst cells occur once every ten cells along the filament [6]. The process takes about twenty hours, during which time, the cell loses its ability to photosynthesize, gain the ability to fix nitrogen and grow a second membrane in order to protect the cell from oxygen entering the cell and inactivating the nitrogenese enzyme [13]. This transformation enlarges the cell to roughly twice the size of a vegetative cell [14]. In gaining the ability to fix nitrogen, the heterocyst can provide nitrates other cells in its filament, although heterocyst now depends on neighboring cells for their sugars created though the photosynthesis process [18]. It should be noted that in the absence of a

combined nitrogen source that the algae will die without the sharing of specially cultivated resources from both vegetative and heterocyst cells. A filament of all vegetative or all heterocyst cells is detrimental and will lead to its collective death. Some combination of the two cell types is necessary if a colony is to be capable of surviving in a combined nitrogen poor environment.

Now the question becomes, what frequency of heterocyst formation in the filament will be most beneficial to the colony [19,20]? This thesis work begins to explore this question through mathematical modeling. Using a system of differential equations to simulate the interplay between vegetative and heterocyst cells and their food sources, the optimal balance for growth has been explored.

Chapter Two: Modeling the Effects of Fluctuation on the Growth Kinetics of the Cyanobacteria *Anabaena* sp.

A simple mathematical model was created through the use of differential equations to simulate the rate of growth, decay, and nutrient usage of the colony. Initially three terms were defined to characterize vegetative cell population. These terms were the broken down into secondary terms in order to accommodate the inclusion of the heterocyst cell type along. The nutrient term was further detailed to specify a differentiation between nitrates from both an atmospheric source versus a media source and minerals. Uniform distribution noise terms were then added to the model to characterize fluctuations within colony population. The mathematical models were created in Mathematica Version 8.0. Four differential equations were created to simulate the basic behavior in *Anabaena* cpcc 387. Specifically, the equations model the growth and decay of the colony as it consumes resources. The first of these equations "*V' [t]"*, is the rate of population change of vegetative cells in the colony. The second, "*H' [t]"*, is the rate of population change for heterocyst cells. The third and fourth equation "*Zm' [t]"* and "*Zn' [t]"*, simulate the rate of availability of minerals and nitrogen in the colonies available environment respectively. "pd" represents the population death rate. "pv" and "ph" represent the population growth rate of the vegetative and heterocyst cells respectively. "pm" and "pn" represent the consumption rate per cell.

"*min_repl*" stands for the rate of mineral replenishment into the environment. This term was included to account for the media that was injected into the batches to account for the amount of sample was taken. "*pnFix*" serves a similar purpose as "*min_repl*" but differs in which it stands for the amount of atmospheric nitrogen available to the heterocyst cells for nitrogen fixation through the constant supply of air given to the batches. "*cf*" is a consumption factor for how readily the vegetative cells can consume the nutrients in their environment. The "*SquareWave*" function accounts for the diurnal environment the cells were incubated in. When the "*SquareWave*" function is coupled with the nutrient intake, the combined terms come to represent the photosynthetic energy creation and reproductive capacity of the colony in a day/night environment. Lastly "*rand1*" and "*rand2*" are terms added to account for noise and fluctuations in the growth of the colony. "*rand1*" specifically is the noise added for the decay of the colony while "*rand2*" is the noise that benefits the population of the colony. "*rand3*" and "*rand4*" serve identical purposes but function in respects to the heterocyst population.

$$V'[t] = -\mathrm{p}_d V[t] + \mathrm{p}_v V[t]\frac{(\mathrm{Zm}[t] * \mathrm{Zn}[t])}{(\mathrm{Zm}[t] + \mathrm{Zn}[t])}\mathrm{cf} * \mathrm{SquareWave}[\{0, \mathrm{li}\}, .5\ t]$$
$$- \mathrm{rand}_1[t]\mathrm{p}_d V[t] + \mathrm{rand}_2[t]\mathrm{p}_v V[t]$$

$$H'[t] = -\mathrm{p}_d H[t] + \mathrm{p}_h V[t]\mathrm{Z}_m[t] - \mathrm{rand}_3[t]\mathrm{p}_d H[t] + \mathrm{rand}_4[t]\mathrm{p}_h H[t]$$

$$\mathrm{Z}_m{}'[t] = -\mathrm{p}_m(V[t] + H[t])\mathrm{Z}_m[t] + \mathrm{min}_{repl}$$

$$\mathrm{Z}_n{}'[t] = -\mathrm{p}_n(V[t] + H[t])\mathrm{Z}_n[t] + \mathrm{p}_{nfix}H[t]$$

Mathematical models have been able to replicate the growth curve patterns found in experimental growth curve data (Fig. 1). When the growth data for batch 1-9 were averaged and then correlated to the model, a correlation coefficient of 0.98 with an error of 2.9% was found (Fig. 2).

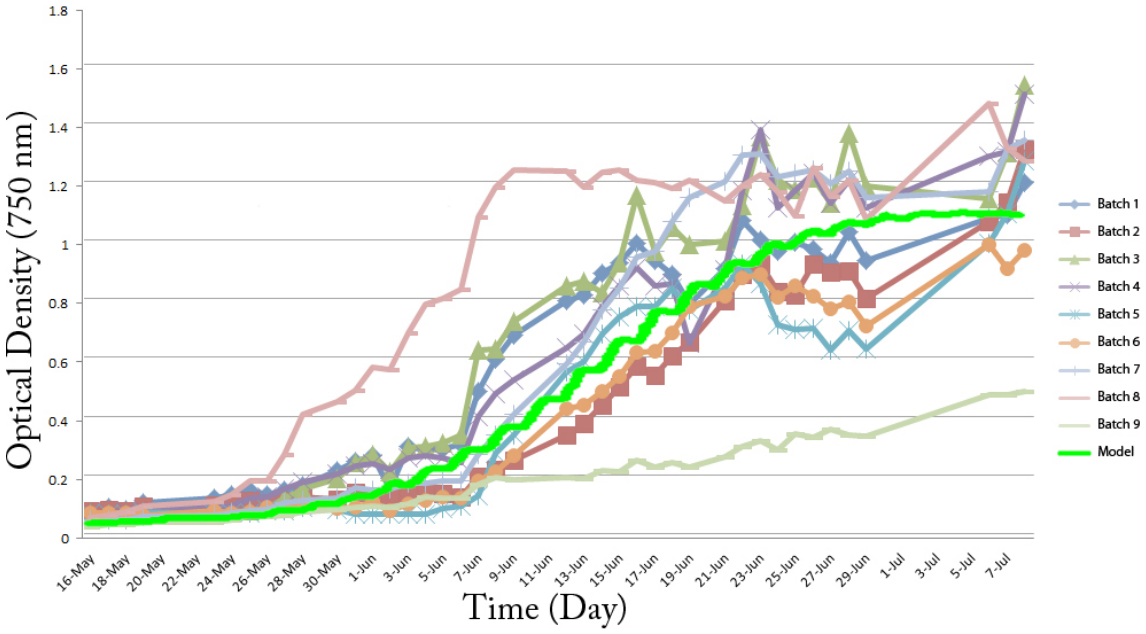

Figure 1: The green curve is the population model of the colony. All other curves are experimental data measured with a spectrometer at 750 nm.

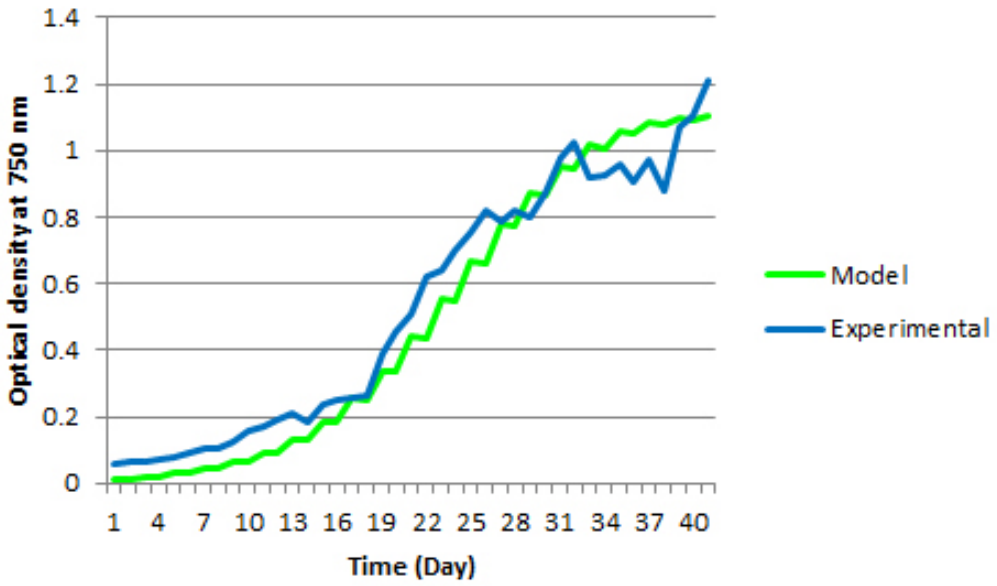

Figure 2: The green curve is the population model of the colony. The represents the average optical density of batches 1-9. Performing a linear correlation test upon the two curves yields a correlation coefficient of 0.98.

The addition of uniformly distributed noise had little effect to the model pre-stationary phase. Once the stationary phase is arrived at, fluctuations become apparent in affecting what OD the colony reaches final stability provided that the noise does not cause the colony to fail entirely. A failed colony is described as reaching a vegetative cell population of zero. The models have been used to simulate the result of a colony under stress both with and without heterocyst cells and with and without noise. The availability or absence of heterocyst cells was chosen as a stressor on the system to allow predictions to be made of the model population as it reached stationary phase. Noise was then added to the model in order to observe effects on the population stability. Noise was defined as a term that effect the population of the colony by varying values, which constructively or destructively affect the other growth and decay terms. The values for the noise amplitude varied unbiased and uniformly between preset

parameters in a random fashion. Setting initial conditions to a nitrate poor environment allowed the model to reveal where the colony either fails or come to a decayed stationary phase after reaching a maximum attainable population. In the simulations where no heterocyst cells were present, the colony failed due to a lack of a nitrate source; when noise was included, it had the effect of crashing the colony sooner than would otherwise have occurred.

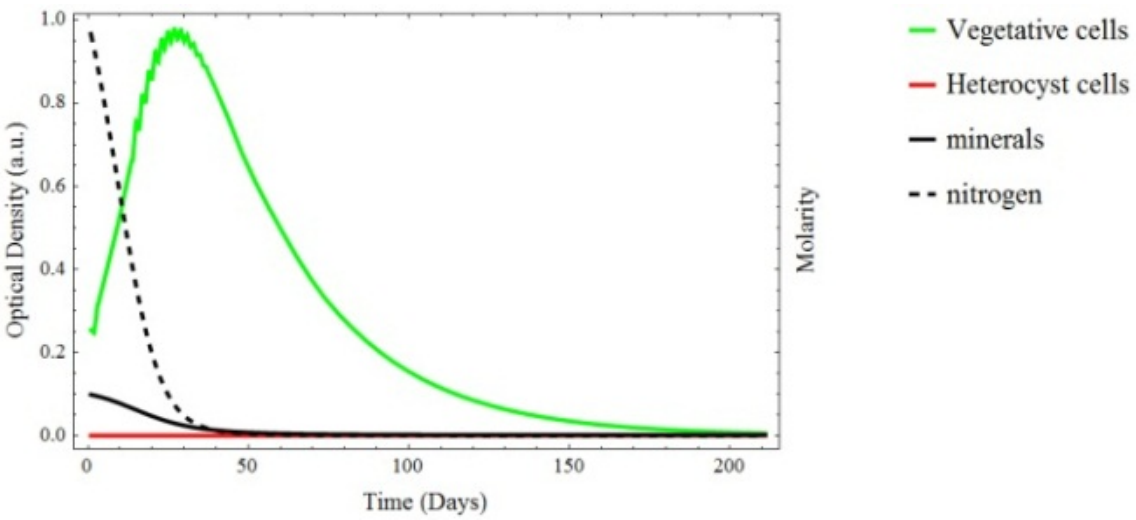

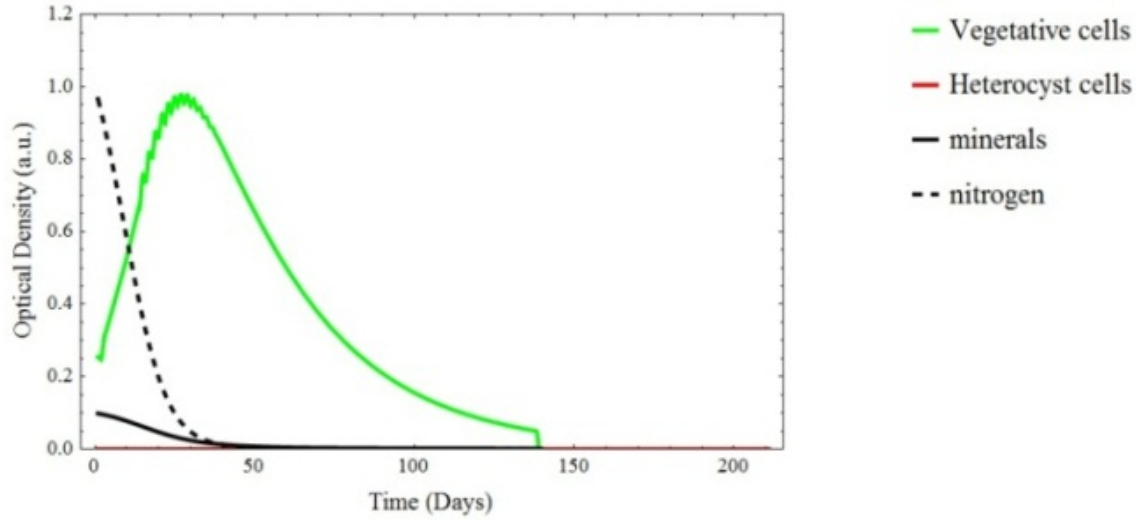

Figure 3 & 4: Fig. 3 (Top) show the simulation run without noise. Fig. 4 (bottom) show a representative run where noise has been introduced into the simulation and the colony has failed.

In the simulations where heterocyst cells were allowed to form, the simulations reached a stationary level lower than the max population attained. This is in part due to the suboptimal level of nitrates available. When noise was introduced to the simulation with heterocyst cells present, the colony reached a similar stationary phase to that reached by the simulation without noise with a notable exception that the colony was now capable of failing.

Mathematical modeling has yielded simulations that have reproduced the growth curves observed in experimental data (Fig. 1) and yielded a correlation to the averaged experimental data of 0.98 (Fig. 2). Further accurate depictions of noise may be achieved by including distinct terms for noise derived from stochastic sources the cells experience.

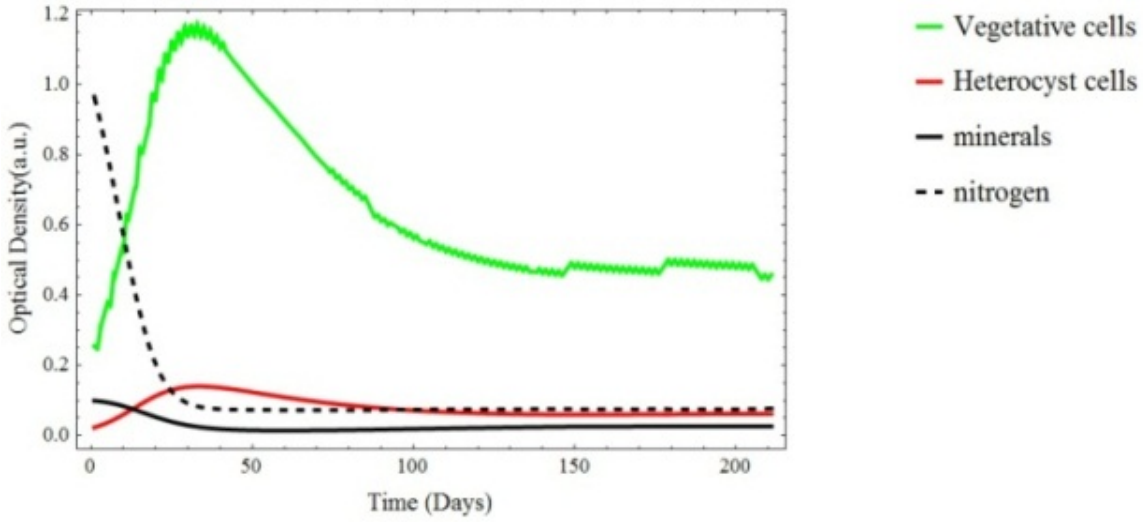
Optical Density(a.u.)
Time (Days)
Vegetative cells
Heterocyst cells
minerals
nitrogen

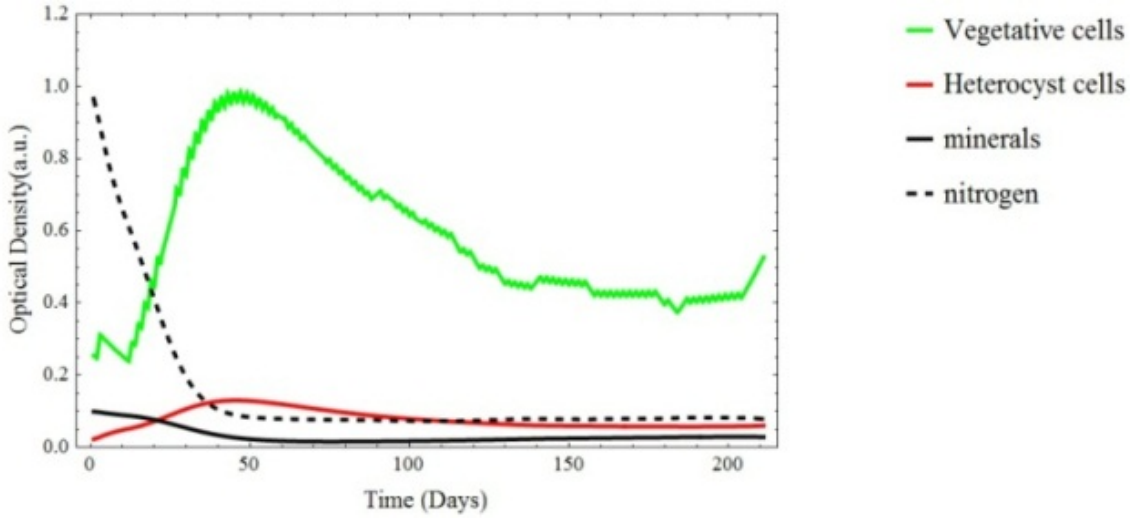
Optical Density(a.u.)
Time (Days)
Vegetative cells
Heterocyst cells
minerals
nitrogen

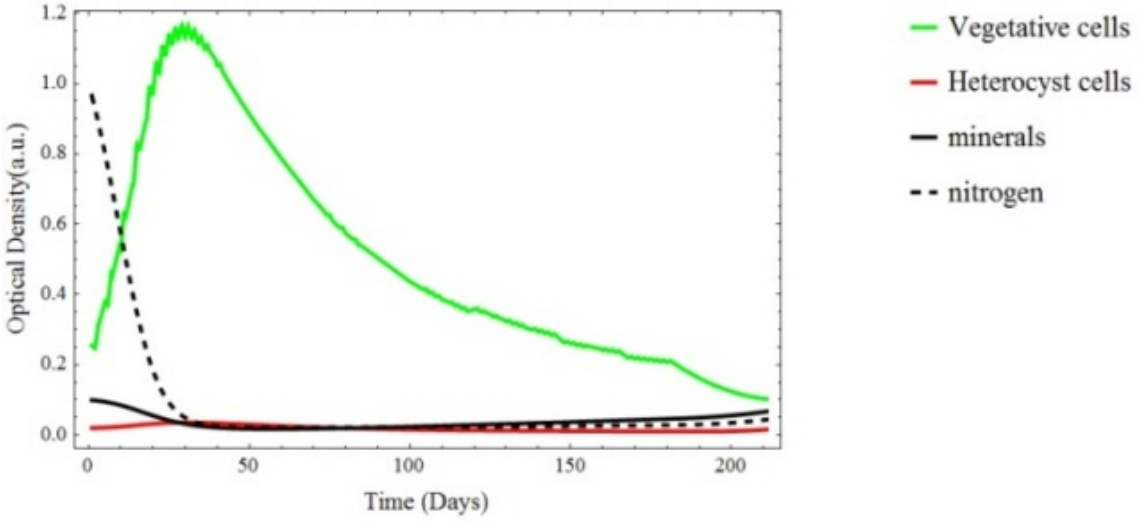
Optical Density(a.u.)
Time (Days)
Vegetative cells
Heterocyst cells
minerals
nitrogen

Figure 5,6 &7: Fig. 5 (top) show the simulation without noise. Fig. 6 (middle) show a representative run where introduced noise has had a positive impact on the colonies population. Fig. 7 (bottom) show a representative run where introduced noise has had a negative impact on the colonies population and has nearly caused it to crash.

Chapter Three: Characterizing the Mechanical Properties of the Phytoplankton *Tetraselmis* via Atomic Force Microscopy

Tetraselmis is a green, single celled alga of the Chlamydomonadaceae family. Tetraselmis is similar to other algae in that it can photosynthesize, but what makes it an interesting candidate for biofuel production is its high lipid concentration. The interest in finding a method to characterize cell elasticity lies in the need to quantitatively characterize how difficult it may be to extract lipids from high lipid producing cells through compromising the cells' membrane. A layer of distinct scales made mainly up of acidic polysaccharides overlap and combine together to form a cell wall called the Theca [21,22].

It is this surface, which the AFM tip first interacts when force curve measurements are performed. If the cell is not ruptured, the force curve attained can be used to find the Young's modulus of the cell.

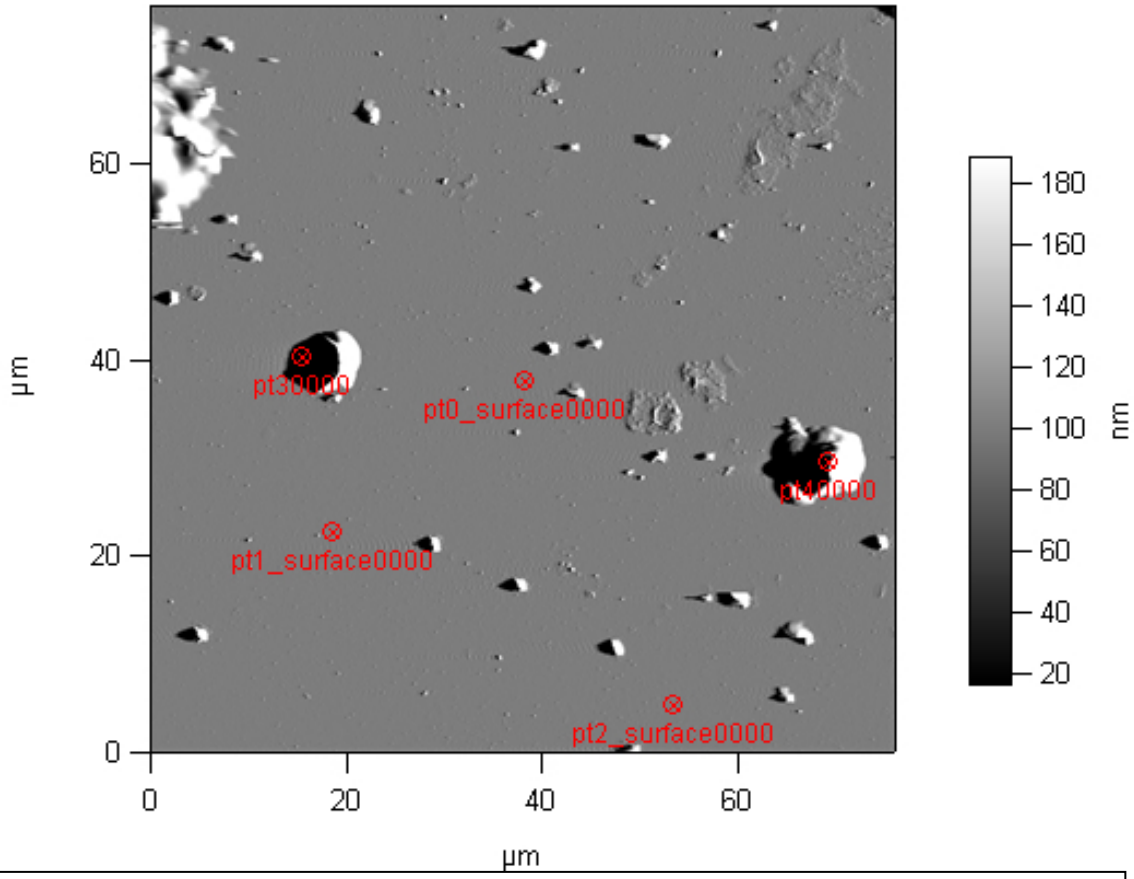

Figure 8: Contact scan of *Tetraselmis* cells affixed to a glass slide via poly-l-lysine. Test point 1, 2 and 3 were performed on the surface vacant of apparent obstructions for calibration and control purposes. Test points 3 and 4 correspond to cells that were tested for elasticity measurements.

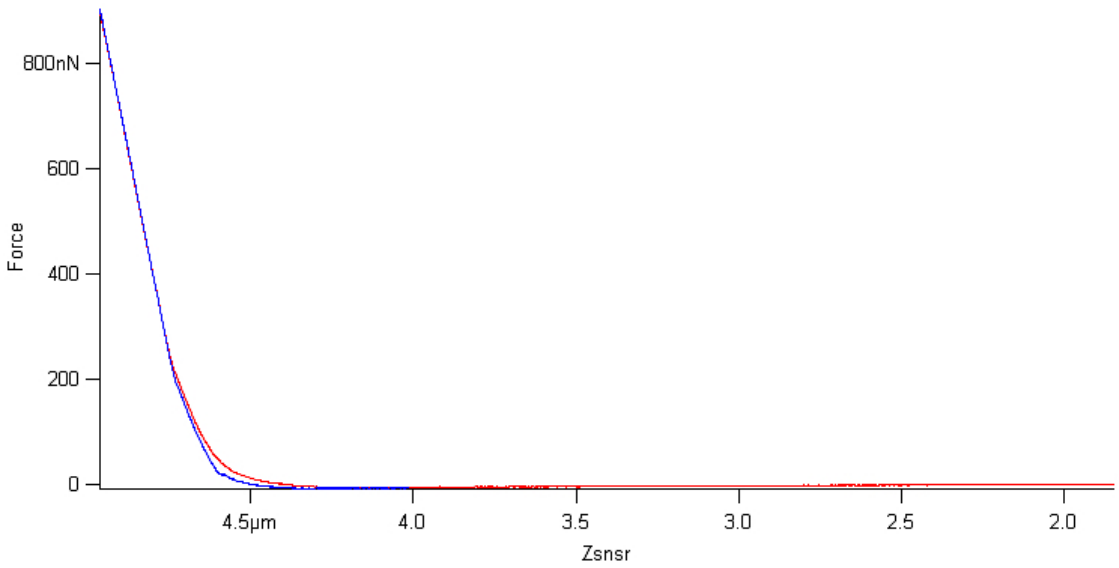

Figure 9: Scan point 3 in Fig. 8. The red line is the tip engaging with the sample until the trigger point is met. The trigger in this image has been set to 900 nN. The blue line is the force felt during the retraction of the probe from the cell. The distance along the x axis is measured relative to where the probe was positioned at initiation of the scan.

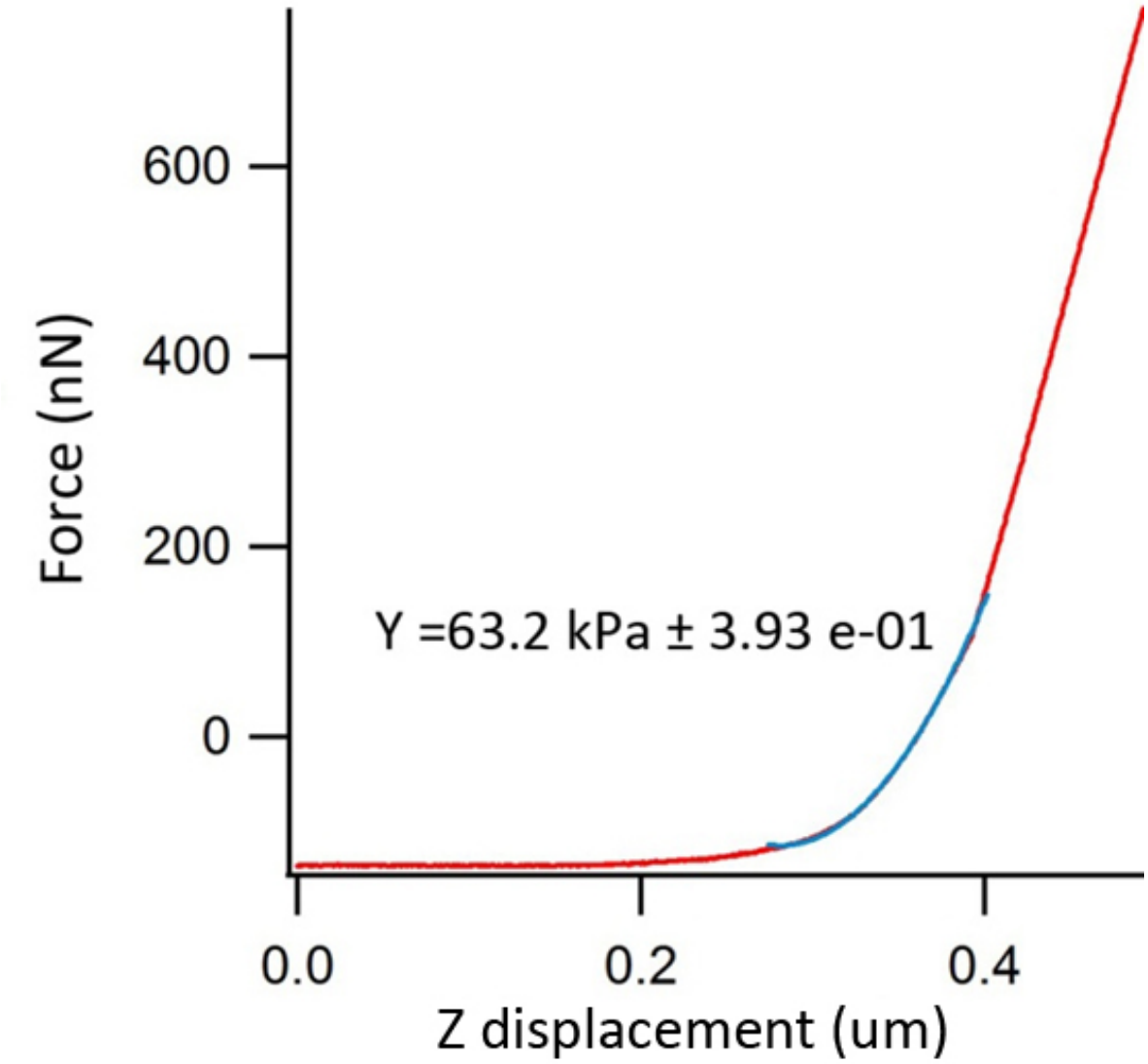

Figure 10: Force curve of pt 3, scan #3 illustrating only the tip engagement and model fit. The red line indicates the engagement of the tip to the cell. The blue overlapping line indicates the curve fit of Sneddon's variation on Hertz model that was used to approximate Young's modulus for *Tetraselmis*.

Sneddon's variation on Hertz model was used as it assumes a cone tip on a probe [7, 8]. The original Hertz model assumed a semispherical shaped tip. "V_{sample}" is the Poisson ratio of the cell. A Poisson's ratio value of rubber, 0.5 is assumed for this ratio as the actual stretching and compression of the cell was indeterminable with available equipment. A is the half angle of the tip. *f(h)* is the force applied at a given distance from the point of initial contact.

$$E_{sample} = \frac{\pi}{2}\frac{f(h)(1 - V_{sample}^2)}{h^2\, Tan(\alpha)}$$

Using the above equation perform a curve for four curves gathered on test point 3 and eight curves gathered on test point 4, we find the average value of Young's Modulus to be 79.8 KPa ± 2.7e-01 for test point 3 and 46.9 KPa ± 5.4e-01 for test point 4.

During engagement, if the cell membrane is compromised, the force curve exhibits a change in slope. This change in slope is attributed to a change in the interface between the tip and the cell membrane. This is concluded to be a rupture of the cell membrane caused by the probe's tip.

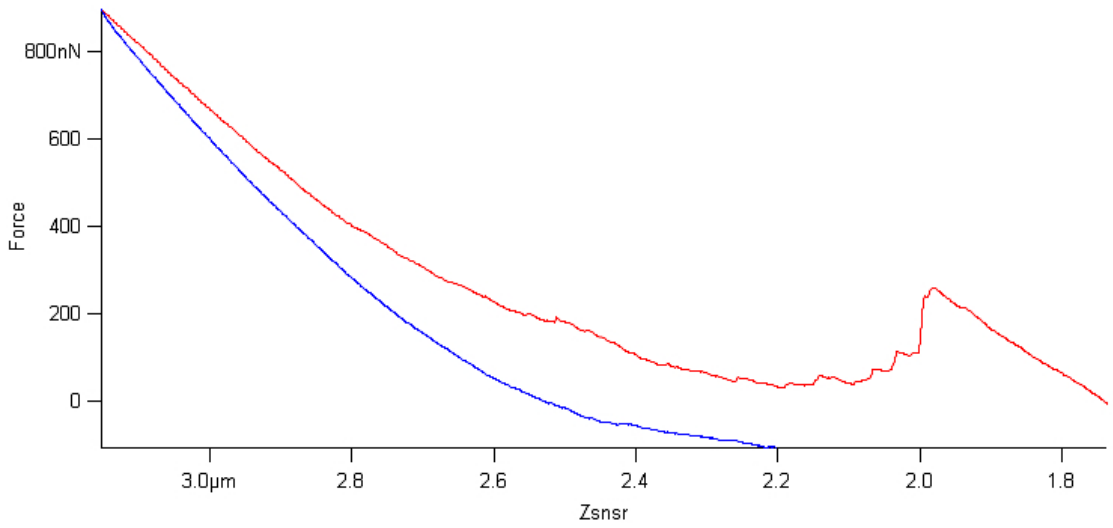

Figure 11: The red line is the tip engaging with the sample until the trigger point is met. The trigger in this image has been set to 900 nN. The blue line is the force felt during the retraction of the probe from the cell. The change in slope is indicative of a change between the membrane tip interactions where a cell rupture is believed to have

After this event, an increase in slope will occur again until the trigger point has been met. The increase in slope is due to the tip puncturing through the cell to the glass surface beneath while force is continually applied until the trigger point is met. During retraction from the cell force curve measurements, it is typically found that the force dips below zero and thus yield a negative force implying that the probe is experiencing a downward pulling force. These forces are understood to be adhesion interactions from the binding of proteins of the cell to the probe's tip.

Force curve measurements yielded data that allowed for calculating Young's modulus of the cell membrane. Young's Modulus was estimated to be an average of 79.8 KPa ± 19.8 for test point 3 and 46.9 KPa ± 2.04 for test point 4 for the *Tetraselmis* cells shown in Fig. 8.

A method for cell immobilization similar to the one discussed in Appendix 3 without the substitution for de-ionized (Di) H_2O would be preferable as the Di H_2O could have an effect on the cell membrane and thus the Young's modulus found. While the current method used mitigates the issue of particulate settling over cells thus decreasing resolution during scans, a method utilizing the native media to the algae would remove a variable introduced when replacing it with Di H_2O. Use of and sampling of various tips with different force constants are suggested when performing force curve measurements on cell membranes. Higher sensitivity can be when using a tip with a lower force constant but runs the risk of the tip breaking more easily. On the other hand, using a tip with a higher force constant has a lower chance of breaking during a measurement but in exchange sensitivity is lost. Trial and error may be required when finding a probe with a suitable force constant for studying cell membranes.

Chapter Four: Overall Conclusions and Future Directions

The mathematical model was able to simulate the behavior of the experimental growth curves successfully (see Fig. 1). The addition of noise was most pronounced in the model after the stationary phase was reached, although relatively smaller fluctuations are seen such as a change in peak OD reached and the time at which this peak occurs. This mathematical model allows for simple predictions of colony growth. With modifications, this model can be adapted to model other bacterial growth including but not limited to other algal candidates for renewable energy and multi-strain colonies incubating and interacting in a single batch. Future directions with the modeling entail modification of the differential equations to include cell signaling and modification of existing umbrella terms in order to specify individual components such as the individual ingredients that compose the minerals in BG-11. The mathematical modeling simplifies fluctuations to generalized noise terms. Simplified into these terms is the quorum sensing that regulates gene expression between the single cell and neighboring cells. Stochastic noise is also simplified into the overall noise term which could affect reproduction of cells. The minerals term can also be further broken down into its base components that are listed in the ingredients list for BG-11. Another simplification that can be broken down is the light received by the cells. Currently a binary “on/off switch” is used to determine day and night but a value that would allow a

gradient of intensity and wavelengths would allow for testing of preferred light sources. An avenue of application for the mathematical modeling that has not been explored yet by the author would be in finding what the optimal vegetative to heterocyst ratio is for maximal colony growth under nitrate poor conditions. Future directions include the creation of a separate set of differential equations that model a different algae and then merging the 2 sets of equations and algae into a shared environment in order to observe and model the cooperation/competitiveness of a multi-strain culture.

The AFM force curve measurements were found to yield reproducible force curve data when tested both on surfaces and on *Tetraselmis* cell membranes. Having reproducible method to characterize membrane elasticity allows for the same algae under different treatments and different algae to be compared directly at how difficult lipid extraction may be. From those lipid producers, strains with or without pretreatments can then be chosen for further study in renewable energy production through lipid to biofuel production. Future interests with cell membrane elasticity modeling include taking multiple measurements on cells during the colonies different stages of growth in order to investigate if any variance in cell elasticity can be seen.

The photobioreactor allowed a simple and efficient chamber to incubate algae in that allows for changes in its environmental conditions in order to allow for a wide range of bacteria. The ability to incubate algae in a simple low maintenance photobioreactor allows for small scale-studies to be carried out on various candidates to renewable energies before scaling up is performed. This allows various smaller tests to

be conducted before investment in larger ventures is pursued. While the photobioreactor was shown to be effective in successfully incubating *Anabaena* and maintaining other strains of algae, it should be noted that media and careful attention to the initial conditions be carefully set and monitored. One of the largest sources of batch failure resulted from batch contamination in with an invasive bacteria would spread and presumably starve the host algae. Other points of concern are careful monitoring of the pH in each of the batch [23]. Having an appropriate amount of buffer in the media helps to mitigate the occurrence of pH swing. Supplying too much CO_2 can also have a negative effect on the stability of the pH in a colony. Possible improvements to the photobioreactor include an automated system to regulate temperature and monitor pH. The inclusion of a custom designed laser array could allow for a method to perform OD readings without the need to take batch samples.

Works Cited

[1] Beal, Colin M., et.al. “Comprehensive Evaluation of Algal Biofuel Production Experimental and Target Results.” Energies 5:6 (2012): 1943-1987.

[2] Vardon, Derek R., et.al. “Thermochemical Conversion of Raw And Defatted Algal Biomass Via Hydrothermal Liquefaction and Slow Pyrolysis.” Bioresource Technology 109 (2012): 178–187.

[3] A.A.Tsygankov, et.al. “Hydrogen Production by Cyanobacteria in an Automated Outdoor Photobioreactor under Aerobic Conditions.” Biotechnology and Bioengineering 80:7 (2002): 777-783.

[4] Najafi, Gholamhassan, et.al. “Algae as a Sustainable Energy Source for Biofuel Production in Iran: A Case Study.” Renewable and Sustainable Energy Reviews 15 (2011): 3870–3876.

[5] Cornelissen, Stijn, et.al. “The Role of Bioenergy in a Fully Sustainable Global Energy System” Biomass and Bioenergy 41 (2012): 21-33.

[6] Rippka, Rosemarie, et. al. "Generic Assignments, Strain Histories and Properties of Pure Cultures of Cyanobacteria." Journal of General Microbiology 111 (1979): 1-61.

[7] Demirbas, M. Fatih, et.al. “Biofuels from Algae for Sustainable Development.” Applied Energy 88 (2011): 3473–3480.

[8] Zhu, J. Y, et. al. "Conceptual Net Energy Output for Biofuel Production from Lignocellulosic Biomass through Biorefining." Progress in Energy and Combustion Science 38:4 (2012): 583-598.

[9] Jones, Carla S., et. al. "Algae Biofuels: Versatility for the Future of Bioenergy." Current Opinion in Biotechnology 23:3 (2012): 346-351.

[10] Henson , Brian J., et.al. "Molecular Phylogeny of The Heterocystous." International Journal of Systematic and Evolutionary Microbiology 54 (2004): 493–497.

[11] Valladares, Ana, et.al. "Specific Role of the Cyanobacterial PipX Factor in the Heterocysts." Journal of Bacteriology 193:5 (2011): 1172–1182.

[12] Mariscal, Vicente, et.al. "Multicellularity in Heterocyst-Forming Cyanobacterium Pathways for Intercellular Communication." Advances in Experimental Medacine and Biology 675 (2010): 123-135.

[13] Kumar, Krithika, et. al. "Cyanobacterial Heterocysts." Cold Spring Harb Perspect Biology 2:4 (2009): a000315-.

[14] Nicolaisen, Kerstin, et. al. "The Cell Wall in Heterocyst Formation by *Anabaena* sp. PCC 7120." Journal of Basic Microbiology 49 (2009): 5-24.

[15] Schneegurt , Mark A., et.al. "Oscillating Behavior of Carbohydrate Granule Formation and Dinitrogen Fixation in the Cyanobacterium Cyanothece sp. Strain ATCC 51142." Journal of Bacteriology 176:6 (1994): 1586-1597.

[16] Bothe, Hermann, et. al. "Nitrogen Fixation and Hydrogen Metabolismin Cyanobacteria." Microbiology And Molecularbiology Reviews 74:4 (2010): 529–551.

[17] Haselkorn , Robert, et. al. "A New Player in The Regulatory Cascade Controlling Heterocyst Differentiation in Cyanobacteria." Molecular Microbiology 77:3 (2010): 537–539.

[18] Meeks , John C. , et. al. "Regulation of Cellular Differentiation in Filamentous Cyanobacteria in Free-Living and Plant-Associated Symbiotic Growth States." Microbiology and Molecular Biology Reviews 66:1 (2002): 94–121.

[19] Rossetti, Valentina, et. al. "The Evolutionary Path to Terminal Differentiation and Division of Labor in Cyanobacteria." Journal of Theoretical Biology 262 (2010):23-34. Web.

[20] Rossetti, Valentina, et. al. "Emergent Multicellular Life Cycles in Filamentous Bacteria Owing to Density-Dependent Population Dynamics." Journal of The Royal Society (2011):

[21] Domozych, DS, et. al. "Development of the Cell-Wall in Tetraselmis - Role of the Golgi-Apparatus and Extracellular Wall Assembly." Journal of Cell Science 52 (1981):351-371.

[22] Becker, B., et. al. "Structure, Composition, and Biogenesis of Prasinophyte Cell Coverings." Protoplasma 181:1-4(1994):233-244.

[23] Kaplan, Aaron, et. al. "Photosynthetic Response to Alkaline pH in *Anabaena* Variabilis." Plant Physiol. 67 (1981): 201-204.

Appendix 1: Growth Chamber

The frame of the photobioreactor (PBR) was built from Unistrut. The dimensions of the structure are 29"x28" on the left and right ends, 48"x28" on each side of the front and back and 48"x29" on the top and bottom. The entire frame was wrapped in material, which had a white reflective material on one side.

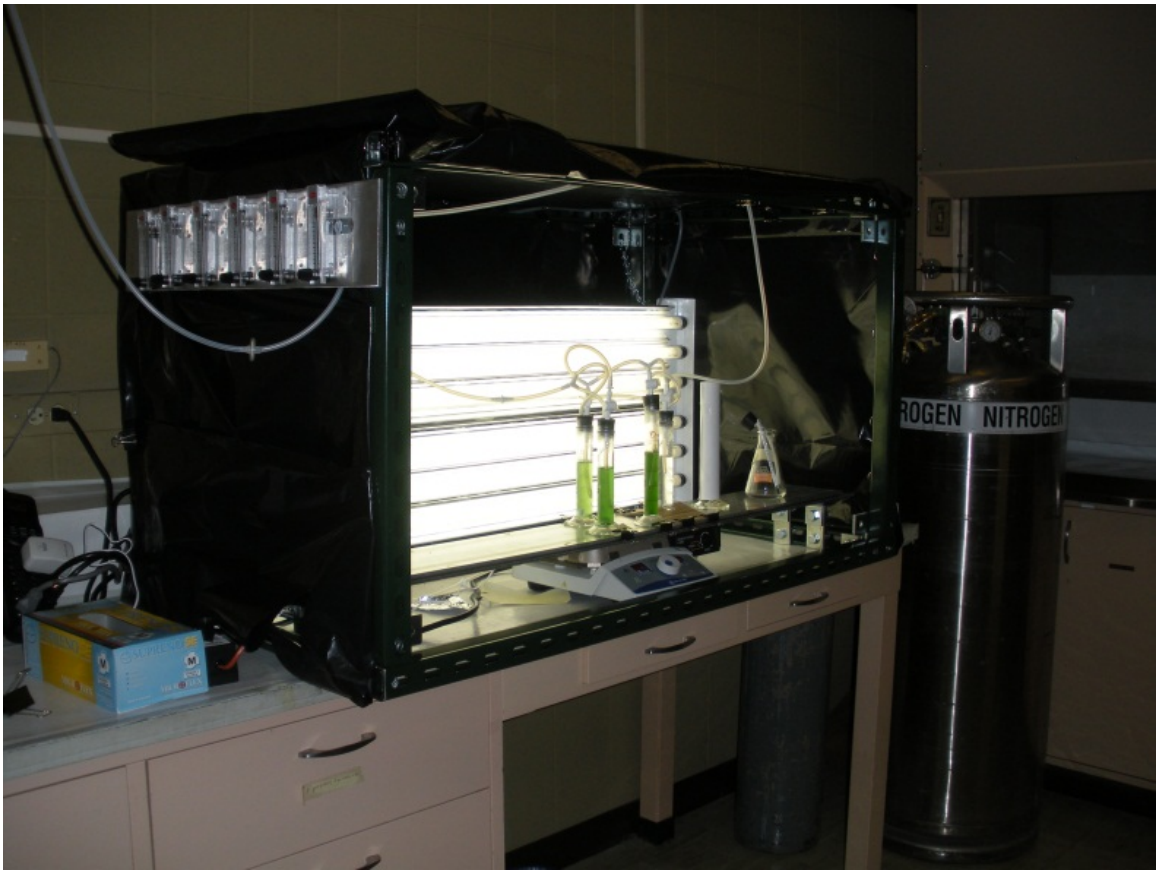

Figure 12: The photobioreactor with flow control valves mounted to the left of the structure.

This reflective surface was placed so as to face the inside of the PBR. All sides were tapped down and sealed save the front, which was allowed to fold back along the topside to allow for human access to the PBR. When access was not necessary, the front access panel was kept closed with Velcro that was tapped to the sides of the panel. A light bank that holds a maximum of 6 florescent light tubes was placed along the back of the PBR. An automatic timer external to the PBR controls the 12 hour on/off cycle of the light bank. A square hole was cut out of the right hand side of the PRB in that a fan was secured to the reflective material to allow for positive pressure in the PBR in order to mitigate outside contaminants from entering. The fan is equipped with a 0.2um filter. 6 flow control valves were affixed to an aluminum plate that was then affixed to the PBR. These flow control valves control the amount of air and CO2 that each of the batches receives individually. 2 aluminum plates rest on the bottom frame of the PBR, raised a few inches from the base. In between the 2 aluminum plates rests induction tape, which is used to obtain higher ambient temperatures within the PBR when needed. Below the aluminum plates are magnetic spin tables that rest directly below each graduated cylinder. Each graduated cylinder is corked with a rubber stopper and further sealed with parafilm. The rubber stopper has 3 holes that run through it. Through the first opening, an inlet tube allows gasses to be deposited into the liquid. The second opening allows gases to be vented out of the graduated cylinder. The third hold has a stainless steel syringe permanently placed in it that allows for samples to be removed from the liquid. Parafilm also covers the opening to the stainless steel syringe when not

in use and is sterilized with Ammonia before and after each use. There are gas filters of pore size .45 um throughout the tubing system. Each cylinder has a filter in the gas intake and exhaust connected to each cylinder. There are also filters placed near the source for the air and CO2. Silicon tubing was cut to accommodate the location of various sources of gas cylinders and air pumps along with numerous smaller sections of tubing, which connect the flow meters to the glass cylinder growth chambers. All equipment that was in direct contact with the algae or was open to spreading contamination to the inside of the glass cylinder growth chambers was thoroughly decontaminated. Decontamination procedures for all glass wear, tubing and equipment is as follows, overnight bath in mixture of 1 parts bleach 9 parts Di H_2O, repeated rinsing's with Di H_2O to remove any residual bleach, autoclaive for a minimum of 30 minutes covered in aluminum foil to prevent contamination once removed from autoclaive, placed in laminar flow hood and exposed to ultraviolet light for a minimum of 1 hour and finally wiped down with 70% ethanol. When connections of tubing were made, all openings and connectors were again wiped down with ethanol.

Appendix 2: Experimental Growth

Anabaena sp. strain cpcc 387 was obtained from the Canadian Phycological Culture Centre. Batches were grown in BG-11 medium with NaCl and buffered with TRIS at 30°C(+-3 °C) in a light intensity of 20K lux in a graduated cylinder.

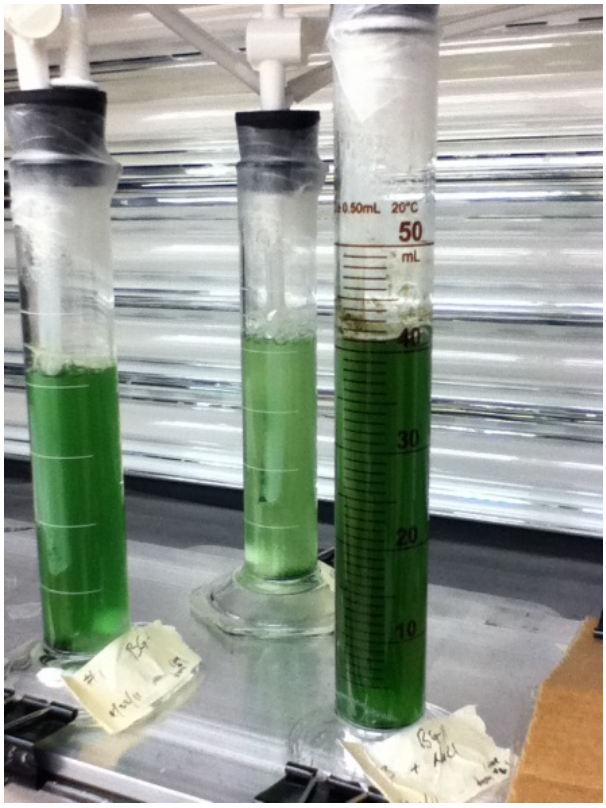

Figure 13: A close up of the glass cylinders used to incubate *Anabaena*.

BG-11 was buffered with TRIS to a pH of 7.5. Each cylinder contained a magnetic stir rod that was spun by a magnetic spin table underneath each cylinder. All batches were grown in a chamber where light was controlled. Light was controlled on a 12 hour on/off cycle to simulate day/night conditions. 0.5ml samples were taken each day to monitor the growth of each batch. The samples taken were checked for optical density (OD) using a Spectrometer at a wavelength of 750 nm. An OD of pure BG-11 media was used to allow for a baseline against which the samples would be compared. A general trend was found during the growth of the colony in each batch. Initial growth proceeded slowly over the course of 1-3 week with little growth shown in a day by day comparison of about an average growth factor of 0.08. This period of growth is typically dubbed the 'lag phase' as it is descriptive of the slow initial growth after inoculation before entering its second distinctive phase of growth. The second phase of growth is the 'exponential phase' in which the colony exhibits a large increase in its growth over a short span of time compared to the 'lag phase'. This period of rapid growth was found for a period of 2-3 weeks in which the size of the colony increased by an average factor of 0.11. The colonies then reach the stationary phase where there is little to no growth after a period of a month after initial inoculation of the batch. After stationary phase, if the colony is not supplied with nutrients or the toxicity of their environment becomes too high, the colony enters a death phase in which the colony can no longer maintain its population.

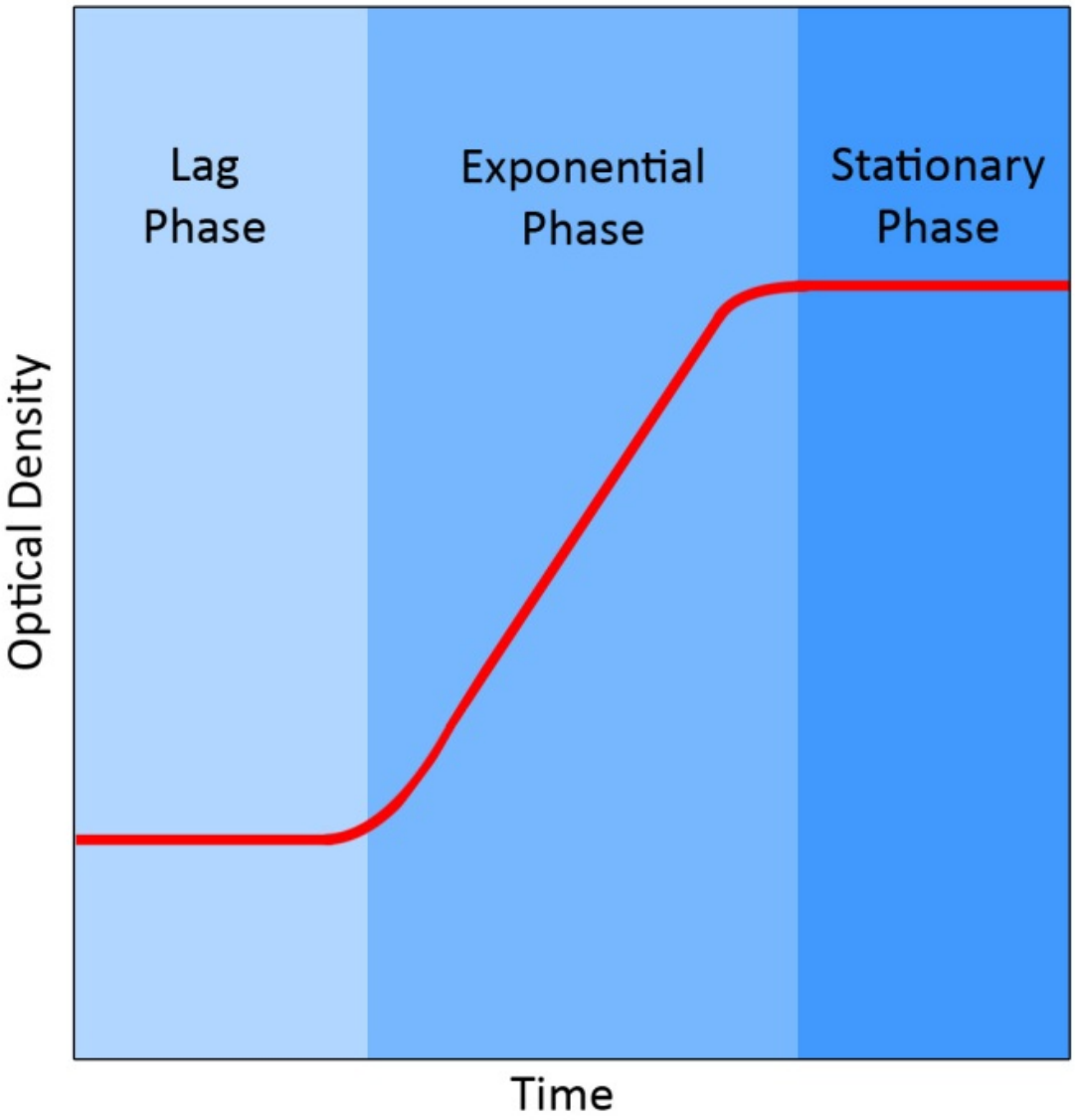

Figure 14: This is a sample growth curve illustrating the initial three growth phases of a colony.

Optical Density @ 750 nm

Date	Batch 1	Batch 2	Batch 3	Batch 4	Batch 5	Batch 6	Batch 7	Batch 8	Batch 9
16-May	0.072	0.079	0.05	0.064	0.068	0.07	0.045	0.053	0.024
17-May	0.088	0.083	0.067	0.07	0.066	0.07	0.048	0.062	0.031
18-May	0.08	0.079	0.063	0.078	0.067	0.069	0.047	0.072	0.03
19-May	0.104	0.093	0.067	0.08	0.074	0.061	0.057	0.093	0.04
23-May	0.122	0.096	0.068	0.092	0.064	0.078	0.062	0.108	0.038
24-May	0.133	0.106	0.075	0.094	0.068	0.071	0.068	0.134	0.047
25-May	0.148	0.112	0.078	0.119	0.068	0.074	0.076	0.179	0.061
26-May	0.134	0.096	0.085	0.125	0.083	0.09	0.08	0.181	0.057
27-May	0.148	0.112	0.12	0.152	0.078	0.09	0.106	0.271	0.06
28-May	0.162	0.125	0.151	0.177	0.09	0.102	0.113	0.407	0.074
30-May	0.213	0.118	0.188	0.203	0.08	0.086	0.122	0.45	0.083
31-May	0.244	0.139	0.243	0.23	0.066	0.089	0.156	0.488	0.091
1-Jun	0.267	0.128	0.271	0.236	0.067	0.11	0.147	0.567	0.093
2-Jun	0.153	0.125	0.212	0.219	0.064	0.076	0.151	0.558	0.089
3-Jun	0.296	0.141	0.291	0.257	0.064	0.101	0.171	0.685	0.1
4-Jun	0.285	0.142	0.297	0.266	0.067	0.111	0.173	0.78	0.124
5-Jun	0.287	0.138	0.308	0.258	0.084	0.125	0.18	0.8	0.121
6-Jun	0.304	0.123	0.335	0.24	0.093	0.119	0.178	0.832	0.121
7-Jun	0.485	0.193	0.624	0.397	0.129	0.181	0.27	1.077	0.169
8-Jun	0.594	0.218	0.628	0.477	0.274	0.212	0.334	1.179	0.192
9-Jun	0.677	0.249	0.723	0.525	0.337	0.264	0.406	1.238	0.184
12-Jun	0.795	0.336	0.843	0.634	0.55	0.424	0.58	1.235	0.191
13-Jun	0.813	0.375	0.858	0.68	0.586	0.438	0.651	1.18	0.186
14-Jun	0.889	0.437	0.819	0.774	0.679	0.484	0.761	1.233	0.216
15-Jun	0.924	0.5	0.924	0.844	0.738	0.537	0.835	1.241	0.211
16-Jun	0.99	0.57	1.152	0.907	0.772	0.618	0.942	1.205	0.248
17-Jun	0.93	0.538	0.962	0.844	0.773	0.622	0.963	1.196	0.226
18-Jun	0.884	0.606	1.044	0.853	0.836	0.683	1.062	1.176	0.243
16-Jun	0.99	0.57	1.152	0.907	0.772	0.618	0.942	1.205	0.248
17-Jun	0.93	0.538	0.962	0.844	0.773	0.622	0.963	1.196	0.226
18-Jun	0.884	0.606	1.044	0.853	0.836	0.683	1.062	1.176	0.243
19-Jun	0.782	0.652	0.983	0.65	0.76	0.774	1.144	1.205	0.226
21-Jun	0.903	0.794	0.997	0.899	0.837	0.807	1.199	1.132	0.26
22-Jun	1.067	0.882	1.119	1.167	0.917	0.87	1.291	1.185	0.295
23-Jun	0.999	0.918	1.353	1.376	0.853	0.884	1.295	1.225	0.316
24-Jun	0.962	0.824	1.205	1.111	0.71	0.806	1.217	1.166	0.286
25-Jun	0.992	0.814	1.171	1.169	0.694	0.845	1.229	1.083	0.341

Optical Density @ 750 nm (continued)

Date	Batch 1	Batch 2	Batch 3	Batch 4	Batch 5	Batch 6	Batch 7	Batch 8	Batch 9
26-Jun	0.969	0.92	1.21	1.226	0.701	0.808	1.239	1.246	0.327
27-Jun	0.922	0.892	1.124	1.124	0.625	0.767	1.193	1.148	0.354
28-Jun	1.026	0.894	1.365	1.203	0.69	0.79	1.234	1.202	0.336
29-Jun	0.931	0.802	1.184	1.11	0.629	0.706	1.145	1.072	0.332
6-Jul	1.074	1.062	1.143	1.286	0.99	0.983	1.166	1.466	0.472
7-Jul	1.087	1.128	1.298	1.302	1.09	0.904	1.311	1.315	0.474
8-Jul	1.196	1.311	1.528	1.498	1.269	0.966	1.339	1.271	0.485

Table 1: Experimental optical density readings at 750 nm wavelength of batch 1-9.

Appendix 3: Atomic Force Microscopy

Tetraselmis, a genus of phytoplankton, was used in the characterization of cell membrane elasticity. *Tetraselmis* was chosen as the candidate for testing due to its high lipid content. The batch of *Tetraselmis* that was received was supplied by NREL. Samples of *Tetraselmis* were prepared for study in the AFM using the following procedure. A sample of 10 mls from a batch is taken. This sample is pelleted down in a centrifuge at 1000 rpm for 10 minutes at a temperature of 20˚C. The supernatant is then removed and replaced with 5 mls of DiH_2O. This is done in order to remove particulate from the sample as they can obscure viewing of the cells during the AFM scan. The sample is then agitated in order to resuspend the *Tetraselmis*. The sample is then pipetted onto 2 glass slides precoated with Poly-L-Lysine. Each slide receives 2.5 mls of the sample and is then kept in a chamber made out of aluminum foil overnight. Allowing the sample to rest on the glass slide overnight gives the cells time to drift to the bottom of the slide adhering to the Poly-L-Lysine. The sample was then washed with DiH_2O to remove cells, which have yet to bind securely to the slide. The slide is then placed in the AFM and hydrated with DiH_2O to prevent cells from drying during the procedure. AFM calibration and scans are carried out under water. Pyrex-Nitride probes (PNP-TR-20) are used for these scans. The cantilevers of length 200 um are chosen for these scans for their low force constant of 0.08 N/m. Scans in contact mode are done until viable cell candidates are found for force curve measurements.

Preferable force curve candidates are cells that are not clumped together and are of the relative size and shape expected for *Tetraselmis* being tested. Once scans are complete and viable cell candidates have been chosen, various single force curve measurements are carried out on vacant, flat areas to provide a control force curve, which to compare cell membrane force curves against. Cells are probed near their center to mitigate pushing of the cell by the probe along the planar direction. Control force curves are found to yield a linear increase of force once the probe has made contact with the surface and continue to increase linearly until the trigger point of the preassigned 900 nN threshold has been met. Once the trigger point is reached, the probe retracts back to its original position. Similar procedures are followed when performing single force curves on cells.

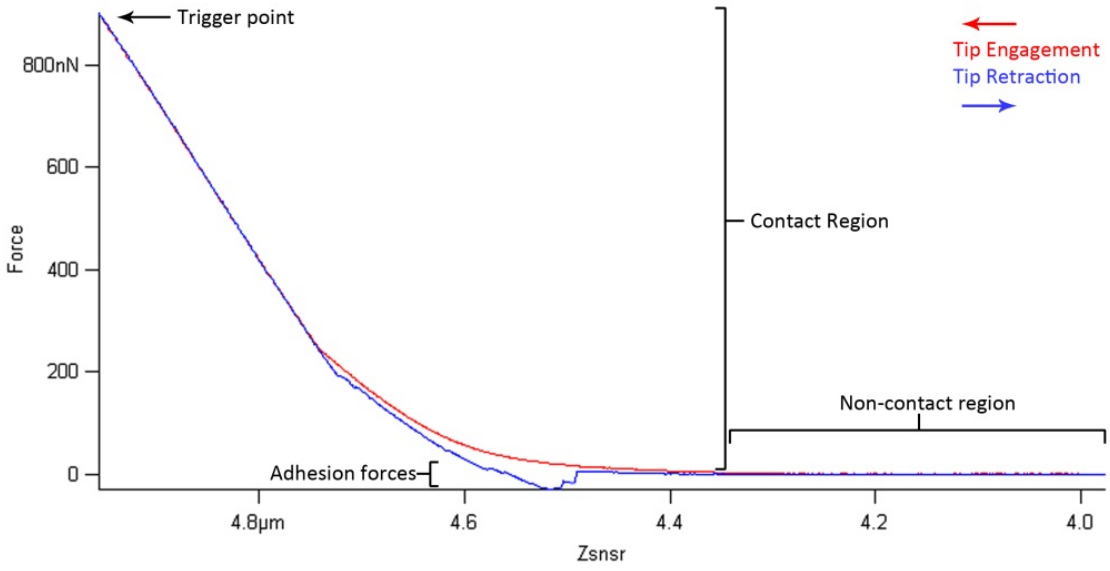

Figure 15: The red line is the tip engaging. The blue is the tip retracting. In the case of cell force curve measurements, proteins from the cell can bind to the tip. Adhesion forces cause the tip to be pulled into the sample during retraction if proteins have bound to the tip.

Appendix 4:

test point 3	Y (kPa)		Error
scan 1	1.39E+02	±	1.5
scan 2	6.21E+01	±	3.22E-01
scan 3	6.32E+01	±	3.93E-01
scan 4	5.48E+01	±	4.97E-01

test point 4	Y (kPa)		Error
scan 1	4.76E+01	±	7.82E-01
scan 2	3.80E+01	±	8.41E-01
scan 3	4.94E+01	±	5.72E-01
scan 4	4.58E+01	±	6.99E-01
scan 5	4.13E+01	±	5.56E-01
scan 6	4.54E+01	±	5.06E-01
scan 7	5.04E+01	±	4.41E-01
scan 8	5.70E+01	±	4.33E-01

Table 2,3: Tables 2 and 3 show the fitted value for Young's modulus using Sneddon's variation on the Hertz model to fit to the experimental force curve obtains. Scans were performed sequentially with a 3 second delay between scans at their respective test points.